Available online at www.sciencedirect.com
ScienceDirect
Trans. Nonferrous Met. Soc. China 27(2017) 1052−1062
Transactions of Nonferrous Metals Society of China
www.tnmsc.cn

Effect of Ce content on mechanical properties of Ce/Cr coated open-cell Ni−Cr−Fe alloy foams

Qiu PANG[1,2], Zhi-li HU[2,3,4], Guo-rong WANG[1]

1. School of Mechanical and Electrical Engineering, Wuhan Donghu University, Wuhan 430212, China;
2. Hubei Key Laboratory of Advanced Technology of Automobile Components, Wuhan University of Technology, Wuhan 430070, China;
3. Hubei Collaborative Innovation Center for Automotive Components Technology, Wuhan University of Technology, Wuhan 430070, China;
4. State Key Laboratory of Advanced Welding and Joining, Harbin Institute of Technology, Harbin 150001, China

Received 1 March 2016; accepted 28 December 2016

Abstract: The Ce/Cr coating was homogenously deposited onto the reticulated open-cell Ni−Cr−Fe alloy foam by the pack cementation process. The mechanical properties of the Ce/Cr coated alloy foams were investigated by the quasi-static compression test. Simultaneously, the deformation and failure mechanisms of Ce/Cr coated alloy foams were discussed. The results show that the adding amount of CeO_2 powders influences the mechanical properties of the Ce/Cr coated alloy foams. Despite an increase in density as compared to the uncoated foams, the Ce/Cr coated foams exhibit improvement in both yield strength and energy- absorption performance. Especially, the energy-absorption performance of 2% Ce/Cr (mass fraction) coated alloy foam is averagely 1.9 times as high as that of the bare Ni−Cr−Fe alloy foam. In addition, the mechanical properties of the Ce/Cr coated alloy foams increase with the increase of strain rate. The distortion and cracking are mainly the deformation behavior of the Ce/Cr coated alloy foam, confirmed by SEM images.

Key words: nickel-based alloy foam; mechanical properties; yield stress; plateau stress; failure mechanism

1 Introduction

Metallic foams have attracted wide range of interest from researchers and industries because of their unique combinations of properties [1]. In recent years, metallic foams serve as lightweight materials for various applications, specifically in the automotive, aerospace, and other high-technology areas [2,3]. At present, of particular interest, open-cell metallic foams have a combination of attractive properties such as permeability, good mechanical properties, thermal and electrical conductivities, and environmental stability [4,5]. However, to date, very few reports exist on open-cell nickel-base alloy foams because of the difficulty of processing these high-melting alloys into foams [6]. In addition, there exist microscopic inhomogeneities such as imperfections, pre-deformed ligaments, and non-planar cell faces. All these factors have an influence on the mechanical performance of open-cell nickel-based alloy foams.

At present, some studies have focused on how to increase the collapse or critical stress of the open-cell metal foams by increasing the material properties of the cell wall. For example, BOONYONGMANEERAT et al [7] demonstrated that the struts of reticulated aluminum foams were coated with nanocrystalline Ni−W by electrodeposition, whose mechanical properties were increased by a factor 2−3 as compared to hypothetical aluminum foam. CHOE and DUNAND [8] reported that the reticulated nickel foams were alloyed with chromium by pack-chromizing, and compressive yield stress of the foam at ambient temperature was in agreement with model predictions. HODGE and DUNAND [9] described that NiAl foams were synthesized from unalloyed nickel foams by using a two-step, high-activity pack-

Foundation item: Project (51501133) supported by the National Natural Science Foundation of China; Project (T201629) supported by the Universities of Hubei Province Outstanding Young Scientific and Technological Innovation Team Plans, China; Project (AWJ-M16-11) supported by the State Key Laboratory of Advanced Welding and Joining, Harbin Institute of Technology, China
Corresponding author: Zhi-li HU; Tel: +86-27-87856773; Fax: +86-27-87856733; E-mail: zhilihuhit@163.com
DOI: 10.1016/S1003-6326(17)60123-7

aluminizing process and these NiAl foams were brittle at ambient temperature, as expected from the very low toughness and ductility of NiAl. However, these studies were limited to the open-cell Al or Ni foam.

The Ni−Cr−Fe system is an important model alloy for nickel-based alloys and austenitic steels because of its good corrosion resistance and high strength at elevated temperatures [10]. Especially, Inconel 690 alloy with the high chromium content (30%) is a high-performance nickel-based alloy used in corrosive and high-temperature environments. Therefore, based on the composition of Inconel 690 (Ni: 60%, Cr: 30%, Fe: 9.5%, C: 0.03% (mass fraction)), the open-cell Ni−Cr−Fe alloy foam is prepared.

The addition of reactive elements (La, Ce or Y) into Cr- or Al-coating has been known to obviously improve the high temperature oxidation resistance and the mechanical properties of the coated alloys [11,12]. Therefore, the Ce/Cr coating is deposited on the surface of the open-cell Ni−Cr−Fe alloy foam by pack cementation. In earlier studies, we studied the oxidation properties of the Ce/Cr coated Ni−Cr−Fe alloy foams [13]. In this work, the effect of Ce content on the mechanical properties of the Ce/Cr coated alloy foams was analyzed by the quasi-static compression test. The results were also compared to the hypothetical Ni−Cr−Fe alloy foam model by Gibson and Ashby theory. In addition, scanning electron microscopy (SEM) was used to investigate the microstructure of the Ce/Cr coated alloy foams before and after the deformation. The deformation and failure mechanisms of Ce/Cr coated Ni−Cr−Fe alloy foams were discussed. Simultaneously, to clearly understand the deformation behavior of the Ce/Cr coated alloy foams, a finite element model was used to simulate the uniaxial compression test of the Ce/Cr coated alloy foams.

2 Experimental

In this work, the substrate material was the reticulated open-cell Ni−Cr−Fe alloy foam, whose composition was 39% Ni, 36% Cr and 25% Fe (mass fraction). The open-cell Ni−Cr−Fe alloy foam was firstly synthesized by co-deposition of Cr and Fe onto open-cell nickel foams after pack-cementation at 1050 °C for 12 h, and then homogenized at 1200 °C for 48 h under vacuum [14]. The geometric parameters of the open-cell Ni−Cr−Fe alloy foam are shown in Table 1.

Table 1 Geometric parameters of open-cell Ni−Cr−Fe alloy foam

Cell diameter/mm	Strut wall thickness/μm	Strut length/mm	Relative density/%
1.25	115±21.5	0.65−0.85	7.8−8.6

The Ce/Cr coated alloy foams with various Ce contents were prepared by the pack cementation process. Firstly, the specimens were cut to a *d*20 mm × 10 mm cylinder shape by DK7716 type electro-discharge machining and ultrasonically cleaned using acetone by KRU−1800 type ultrasonic cleaning machine. A total pack mass of 120 g was poured in a stainless-steel can in which the open-cell Ni−Cr−Fe alloy foam was embedded. The pack compositions of Ce/Cr coatings are shown in Table 2. Then, the sealed can was placed in the rapid heat electric chamber furnace (GWL−1600) at 980 °C for 10 h, followed by air cooling to room temperature. The density of the Ce/Cr coated Ni−Cr−Fe alloy foams was measured by Archimedes method. The mass of the samples was measured using the BP211D analytical balance with an accuracy of 10^{-5} g. The porosity (P) of the samples was calculated by the following formula:

$$P=\left(1-\frac{\rho_{\mathrm{f}}}{\rho_{\mathrm{s}}}\right)\times 100\% \quad (1)$$

where ρ_{f} is the density of the foam material; ρ_{s} is the bulk reference material. Simultaneously, the microstructure and element distribution of the Ce/Cr coatings were analyzed using scanning electron microscope (SEM/EDS, Hitachis−4700). XRD patterns were taken by Rigaku D/max-RB diffractometer with Cu K_{α} radiation. In order to evaluate the mechanical behavior of the Ce/Cr coated Ni−Cr−Fe alloy foams, the microhardness was measured on the cell wall using an HXD−1000 type Vickers microhardness tester with a load of 5 g. In addition, the quasi-static compressive test was conducted in an Instron 5569 testing machine with a cross-head speed of 0.01 and 0.1 mm/s at ambient temperatures. The morphologies and microstructures of the specimens were also examined by S−570/Hitachis−4700 scanning electron microscopy (SEM) after the deformation.

Table 2 Pack compositions of Ce/Cr coatings (mass fraction, %)

Test No.	Al_2O_3	NH_4Cl	Cr	CeO_2
1	73	3	22	2
2	72	3	22	3
3	70	3	22	5

An FE analysis model was created by modeling based on the acquired X-ray CT images. ABAQUS software was used for 2D image processing and FE analysis. The geometric structure parameters of the alloy foams are referred to Table 1. The porous structures comprised of *d*40 mm unit cells were designed with 180 mm in length for each sample. Moreover, an elastoplastic material model was considered with the elastic modulus of 211 GPa, yield strength of 350 MPa,

and Poisson ratio of 0.3.

3 Results and discussion

3.1 Microstructure of Ce/Cr coated Ni−Cr−Fe alloy foams

Figure 1 shows the SEM morphologies of the open-cell Ni−Cr−Fe alloy foam substrate and the Ce/Cr coated alloy foams with 2% Ce and 3% Ce (mass fraction). Figure 2 illustrates typical two-dimensional X-ray CT images of the corresponding specimens. It can

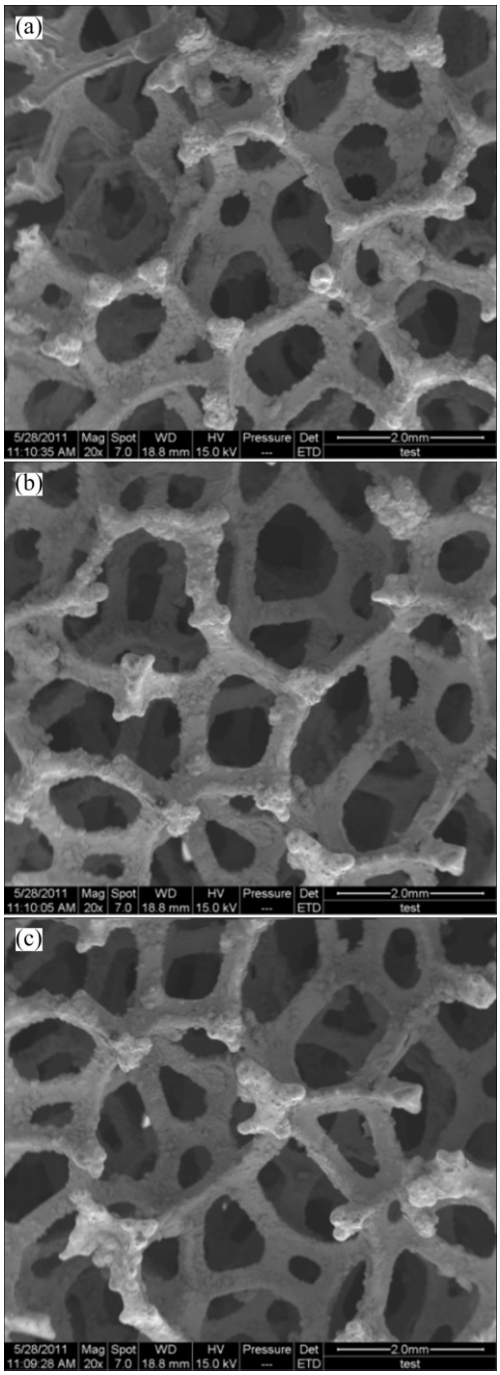

Fig. 1 SEM morphologies of Ni−Cr−Fe alloy foam substrate (a), 2% Ce/Cr coated alloy foam (b) and 3% Ce/Cr coated alloy foam (c)

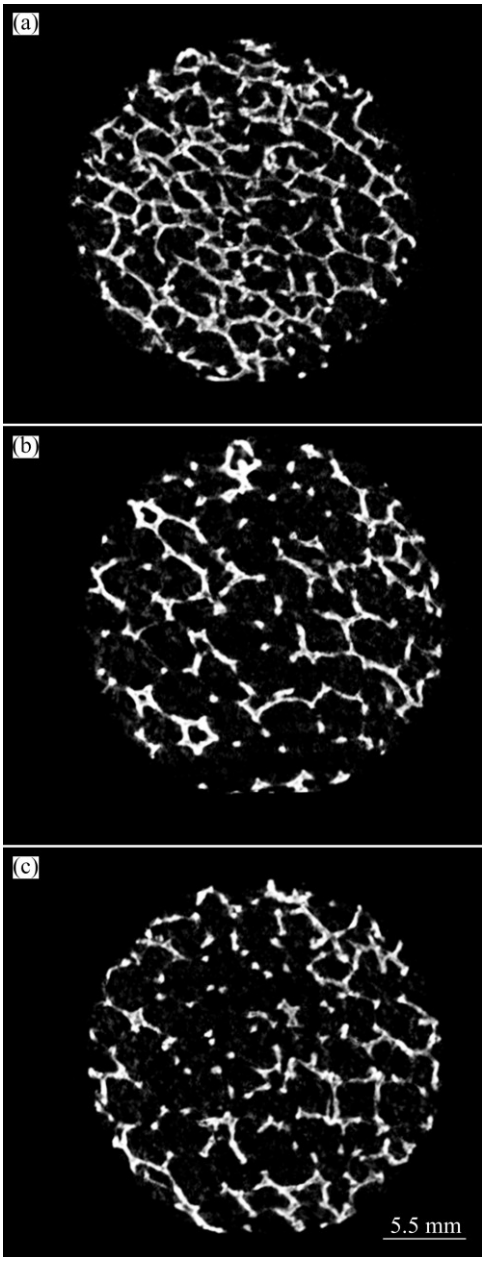

Fig. 2 X-ray CT images of open-cell Ni−Cr−Fe alloy foam (a), 2% Ce/Cr coated alloy foam (b) and 3% Ce/Cr coated alloy foam (c)

be seen that the open-cell Ce/Cr coated Ni−Cr−Fe alloy foams have a complex microstructure consisting of an interconnected network with hollow struts, which keep the original reticulated open-cell Ni−Cr−Fe alloy foam structure in Fig. 1. From a geometric point of view, the Ce/Cr coated Ni−Cr−Fe alloy foam may be regarded as the cell units connected by continuous solid metal ligaments in Figs. 1 and 2. In addition, compared with the Ni−Cr−Fe alloy foam substrate in Fig. 1(a), no macroscopic shape change of the specimens or distortion of the foam cell structure is observed for the Ce/Cr coated alloy foams in Figs. 1(b) and (c).

3.2 Cross-section morphology of Ce/Cr coated Ni−Cr−Fe alloy foams with different contents of Ce

Figure 3 shows the cross-sectional micrographs of the Ce/Cr coated specimens fabricated at 980 °C for 10 h. It can be seen that the Ce/Cr coatings are continuous with a deep grey color. However, the thickness of the Ce/Cr coatings varies significantly with different Ce contents. The thickness of the 1% Ce/Cr coating is not uniform along the Ni−Cr−Fe alloy foam strut, which is about 30 μm in Fig. 3(a). Some voids and cracks exist at the interface between the Ce/Cr coating and the substrate.

Compared with that of 1% Ce/Cr coating in Fig. 3(a), the microstructure of the 2% Ce/Cr coating is more uniform and denser with a total thickness of 35 μm in Fig. 3(b). This is because Ce can accelerate the co-deposition of Ce and Cr, as surface active element [13]. The EDS point analysis of the 2% Ce/Cr coating indicates that the chemical composition of the Ce−Cr coating mainly consists of 90.95% Cr (mole fraction) and small amount of Ni and Fe, which change gradually from the internal section to the surface of the coating in Fig. 3(d). However, as the content of Ce increases to 3%, there are a number of pores at the interface between the Ce/Cr coating and substrate in Fig. 3(c), which may significantly reduce the bonding strength at the interface.

Table 3 lists the geometric structure parameters of the Ce/Cr coated Ni−Cr−Fe alloy foam. For an accurate comparison of experimental results, the cell walls of the open-cell Ni−Cr−Fe alloy foam substrates have the same thickness (125 μm). It can be seen that when Ce content varies from 1% to 3% in the Cr coating, the thickness of the Ce/Cr coatings increases from 30 to 36 μm, and on the contrary, the porosity decreases from 91.6% to

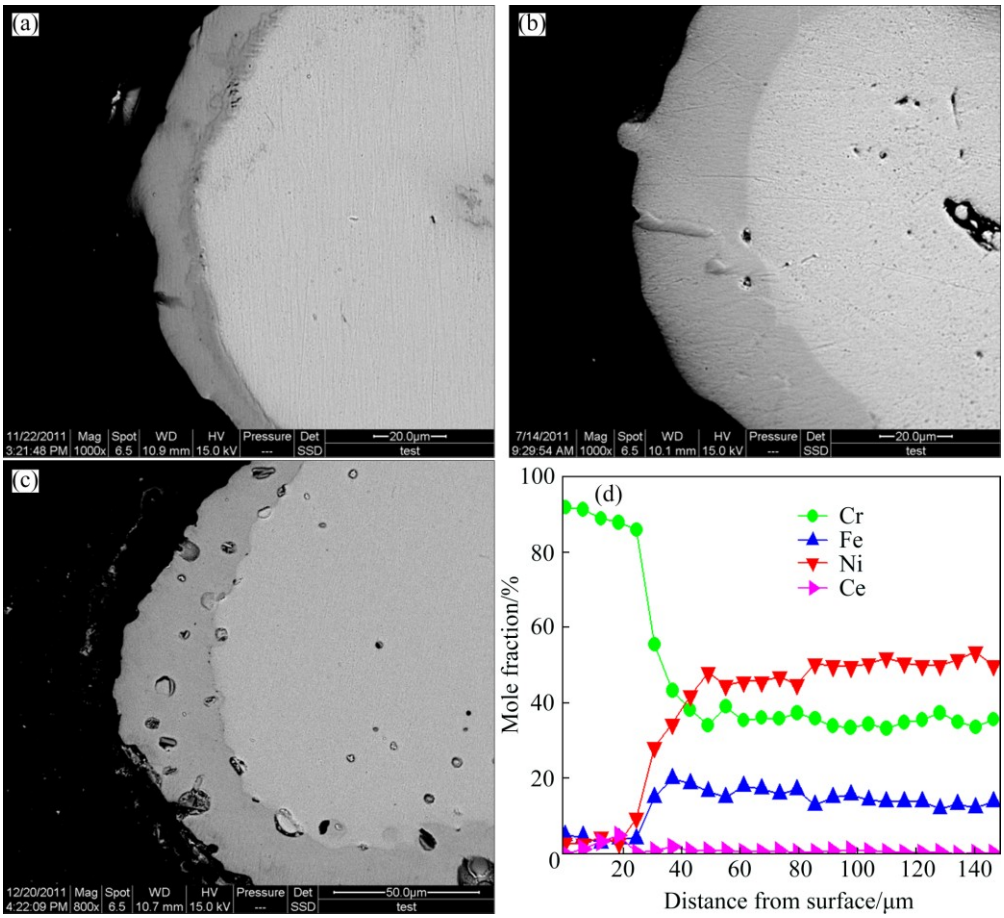

Fig. 3 Cross-section morphologies (a−c) of Ce/Cr coated Ni−Cr−Fe alloy foams fabricated at 980 °C for 10 h and EDS point analysis of 2% Ce/Cr coating (d): (a) 1% Ce/Cr coating; (b) 2% Ce/Cr coating; (c) 3% Ce/Cr coating

Table 3 Geometric structure parameters of Ce/Cr coated open-cell Ni−Cr−Fe alloy foams

Designation	Coating composition	Pore size/mm	Porosity/%	Coating thickness/μm
1% Ce/Cr	1% Ce, Cr balance	1.27	91.6	30
2% Ce/Cr	2% Ce, Cr balance	1.25	91.5	35
3% Ce/Cr	3% Ce, Cr balance	1.25	91.4	36

91.4%. The result suggests that the Ce content is very important for the effective deposition of Cr and Ce in the pack cementation process.

3.3 XRD analysis of Ce/Cr coated Ni−Cr−Fe alloy foams

To verify the existence of phases in the Ce/Cr coated Ni−Cr−Fe alloy foams, Fig. 4 illustrates the XRD patterns of the Ce/Cr coated specimens with different Ce contents. The X-ray analysis indicates the presence of the Cr, (Ni, Cr) and (Fe, Cr) phases in the Ce/Cr coating mainly as Cr phase. This is because the Ce/Cr coating is deposited on the surface of the Ni−Cr−Fe alloy foam, which mainly consists of Cr. Simultaneously, with the increase of Ce content, the peak intensity of the Cr phase increases and the peak intensities of (Ni, Cr) and (Fe, Cr) solid solutions decrease.

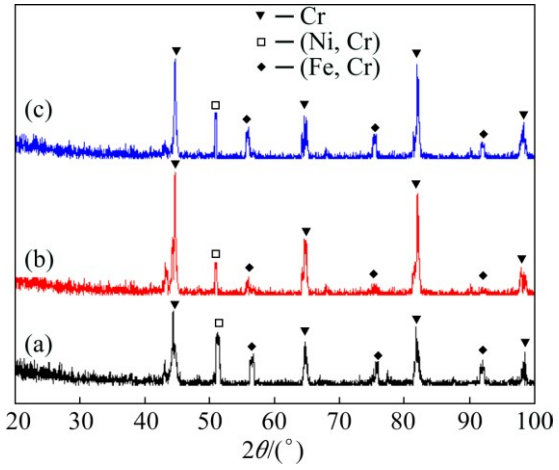

Fig. 4 XRD patterns of Ce/Cr coated Ni−Cr−Fe alloy foams: (a) 1% Ce/Cr coating; (b) 2% Ce/Cr coating; (c) 3% Ce/Cr coating

3.4 Microhardness values of Ce/Cr coated Ni−Cr−Fe alloy foams with various Ce contents

Figure 5 shows the position of microhardness testing point for bare Ni−Cr−Fe alloy foam. Each sample is measured from the marker position (namely, HV_1, HV_2 and HV_3). Figure 6 indicates the microhardness values of the bare Ni–Cr–Fe alloy foams and Ce/Cr coated alloy foams, respectively. The microhardness values of the Ce/Cr coated alloy foams are higher than those of the bare Ni−Cr−Fe alloy foams. With the increase of Ce content from 1% to 3%, the average microhardness value firstly increases and then decreases. Especially, the microhardness value of the 2% Ce/Cr coated alloy foam is almost 1.4 and 1.1 times as high as those of the Ni−Cr−Fe alloy foam and 3% Ce/Cr coated alloy foam, respectively. The results indicate that the addition of Ce leads to the formation of a dense microstructure and improves the strength of the alloy foam struts [15].

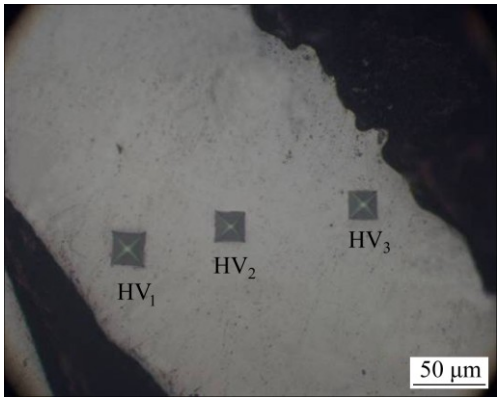

Fig. 5 Position of microhardness test for Ni−Cr−Fe alloy foam

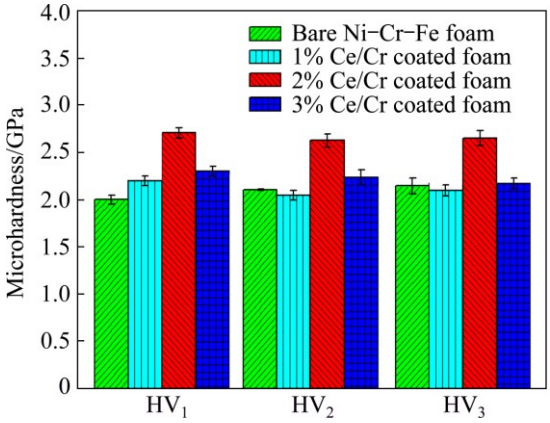

Fig. 6 Microhardness values of Ni−Cr−Fe alloy foams and Ce/Cr coated alloy foams

3.5 Compressive behaviors of Ce/Cr coated Ni−Cr−Fe alloy foams with various Ce contents

Figure 7 shows the typical compressive stress−strain curves of the bare Ni−Cr−Fe alloy foam and the Ce/Cr coated alloy foams at quasi-static strain rate of 0.01 mm/s. It can be seen that all specimens exhibit smooth stress−strain curves that are typical

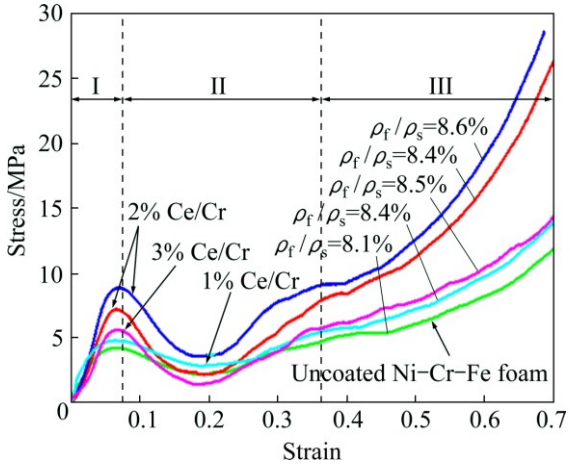

Fig. 7 Compressive stress–strain curves of bare Ni−Cr−Fe alloy foams and Ce/Cr coated alloy foams with various Ce contents at quasi-static strain rate of 0.01 mm/s

characteristics of ductile metallic foam [16]. The addition of Ce increases the compressive strength of the Ce/Cr coated alloy foams obviously. In addition, the uniaxial compressive stress–strain curves of the Ce/Cr coated alloy foams are similar to that of the bare Ni−Cr−Fe alloy foams, comprising three deformation stages: I) elastic deformation stage; II) plateau stage; and III) densification stage [17].

Stage I starts from the beginning of deformation and terminates at the stress peak. The deformation of the alloy foams occurs by elastic buckling, bending and extension of the cell walls [18]. The peak stresses of the Ce/Cr coated alloy foams are in the range of 4.8−8.9 MPa after the onset of yielding. In stage II, the stress acting on the cell walls creates macroscopic plastic deformation in the weak areas of cell walls. The stress decreases with increasing strain and reaches the low valley stress, and then the collapse of the alloy foam occurs. In stage III, a rapid increase in the stress is observed and the successive collapse of the Ce/Cr coated alloy foams occurs.

Simultaneously, compared with the bare Ni−Cr−Fe alloy foams, the Ce/Cr coated alloy foams show significant increase in yield stress and plateau stress. Especially, the yield stress and plateau stress of the 2% Ce/Cr coated alloy foams are 7.2 and 2.3 MPa, 8.9 and 3.5 MPa, which are 1.5−1.7 times and 1.5−2.3 times as high as those of the 3% Ce/Cr coated alloy foams. The increase in strength can be attributed to the increase in the bonding strength between the Ce/Cr coating and the foam substrate.

However, the compressive stress–strain curves of the Ce/Cr coated alloy foams show a very weak stage II in Fig. 7, which are consistent with the results of published literature [19]. This is because the open-cell metallic foam as the substrate is prepared by using the electrodeposition technique. The middle part of the foam skeleton is thinner than the upper and lower surfaces of the foam specimen due to the electroplating conditions. Therefore, the middle part of the foam skeleton will happen to yield under the same loading conditions.

In addition, compared with that of the bare Ni−Cr−Fe alloy foam, the peak stress of the Ce/Cr coated alloy foams is followed by a gradual stress drop. The difference between peak stress and valley stress is 4.2−5.3 MPa. This is because the plastic deformation firstly occurs on the weakest strut of the alloy foams. The Ce/Cr coating strengthens the intensity of the alloy foams, and the compressive stress of the strut of the Ce/Cr coated alloy foam increases. When the struts of cell yield and fracture occur, the stress decreases suddenly from the peak stress to the low valley stress.

Figure 8 indicates the representative compressive stress−strain curves of the Ce/Cr coated Ni−Cr−Fe alloy foams at the strain rate of 0.1 mm/s. It is shown that there are also three regions namely a linear elasticity, a plateau and a densification region in all the curves [20,21]. The yield stress of the Ce/Cr coated alloy foams increases with increasing the strain rate. The yield stress of the 2% Ce/Cr coated alloy foam increases from 7.2 to 8.9 MPa with the same relative density. The yield stress of the 3% Ce/Cr coated alloy foam is increased to 6 MPa at the strain rate of 0.1 mm/s. The results clearly indicate that these alloy foams show sensitivity to strain rate, which are in agreement with the results reported by other authors [22,23].

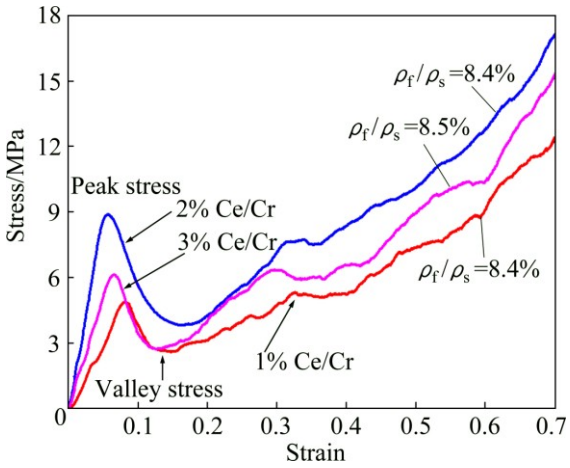

Fig. 8 Compressive stress–strain curves of Ce/Cr coated Ni−Cr−Fe alloy foams with various Ce contents at quasi-static strain rate of 0.1 mm/s

The compressive strength of the open-cell metal foams can be predicted from a simple theory based on cubic unit cells [24]. According to Gibson and Ashby's theory [24], the compressive strength σ_{pl} of hypothetical, uncoated Ni−Cr−Fe foams can be expressed by Eq. (2), as a function of their relative density ρ_f/ρ_s in Fig. 9 (calculated with respect to the density of the solid nickel alloy).

$$\sigma_{pl}=0.3\sigma_{ys}(\rho_f/\rho_s)^{3/2} \quad (2)$$

where σ_{ys} is the yield stress of a bulk reference material. Using values of σ_{ys} taken from Ref. [25], the yield stress of Ni−Cr−Fe alloy is 350 MPa.

Figure 9 indicates compressive strength as a function of relative density for bare Ni−Cr−Fe alloy foam and Ce/Cr coated alloy foams. It is apparent that the Ce/Cr coatings increase compressive strength of the alloy foam as compared with a hypothetical Ni−Cr−Fe alloy foams. Especially, the 2% Ce/Cr coated alloy foam has higher strength than the bare Ni−Cr−Fe alloy foam, 1% and 3% Ce/Cr coated alloy foams. Because it leads to thicker coatings as well as higher intrinsic strength [26]. The results are also consistent with the previous results of microhardness test in Fig. 6.

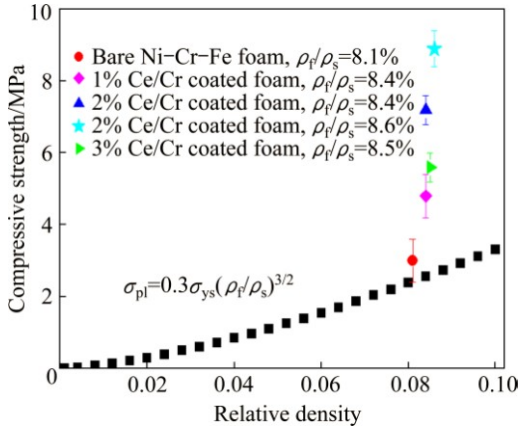

Fig. 9 Compressive strength of Ce/Cr coated Ni−Cr−Fe alloy foams (uncoated Ni−Cr−Fe foam given for comparison) (The error bars are standard deviation determined from duplicate tests. The lines represent the anticipated mechanical response of a hypothetical uncoated Ni−Cr−Fe foam)

In order to prove that the strength enhancement is not caused by an increase in foam density, Fig. 10 presents the specific strength of the alloy foams. The formula is shown below:

$$\sigma_{pl}/\rho_f = 0.3\sigma_{ys}\rho_f^{1/2}\rho_s^{3/2} \quad (3)$$

It is apparent that all Ce/Cr coated alloy foams show higher specific strength than the uncoated Ni−Cr−Fe alloy foam in Fig. 10. Simultaneously, according to the specific strength calculated from Eq. (3), the specific strengths of Ce/Cr coated alloy foams are 2−3 times as high as those of hypothetical Ni−Cr−Fe foam with the same relative density. The result indicates that the Ce/Cr coatings with high bonding strength to substrate increase significantly the mechanical performance of the alloy foams.

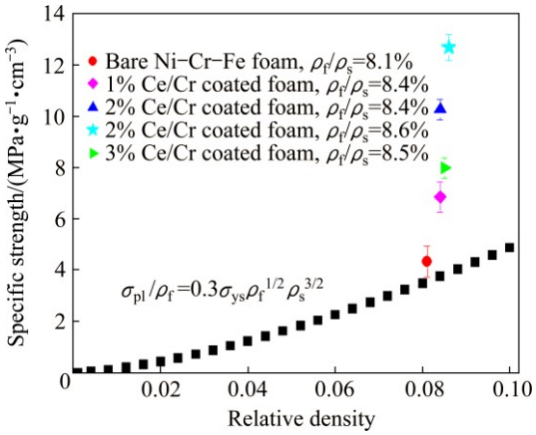

Fig. 10 Specific compressive strength of Ce/Cr coated Ni−Cr−Fe alloy foams (uncoated Ni−Cr−Fe foam given for comparison) (The error bars are standard deviation determined from duplicate tests. The lines represent the anticipated mechanical response of a hypothetical uncoated Ni−Cr−Fe foam)

3.6 Energy-absorption properties of Ce/Cr coated alloy foams with various Ce contents

Energy absorption is an important technological property of the metal foams. The energy absorption per unit volume (W) can be calculated by the area of the stress−strain curves. This can be expressed as follows [27]:

$$W = \int_0^{\varepsilon_d} \sigma(\varepsilon)\mathrm{d}\varepsilon \quad (4)$$

where W is the energy absorption per unit volume; ε_d is the densification strain; σ is the compressive stress when strain is ε.

Figure 11 shows the energy-absorption properties of bare Ni−Cr−Fe alloy foam and Ce/Cr coated alloy foams with various Ce contents, which are calculated according to Eq. (4). It can be seen that the change trend of the energy absorption performance increases linearly with increasing the strain, which is consistent with the change trend of the yield strength in Figs. 7 and 8 . When the yield platform of the samples gradually becomes dense, the energy absorption capacity of Ce/Cr coated alloy foams shows rapid increase between the strains of 0.4 and 0.7. Especially, the 2% Ce/Cr coated alloy foam exhibits the highest energy absorption capacity in all the samples. The energy absorption capacity of 2% Ce/Cr coated alloy foam is averagely 1.9 times as high as that of bare Ni−Cr−Fe alloy foam.

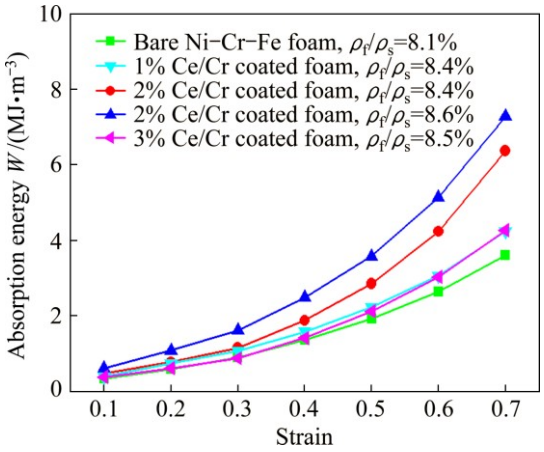

Fig. 11 Energy absorption capability of bare Ni−Cr−Fe alloy foam and Ce/Cr coated alloy foams

Table 4 illustrates the mechanical properties of the bare Ni−Cr−Fe alloy foam and Ce/Cr coated alloy foams with various Ce contents. According to Table 4, it can be seen that the yield stress, plateau stress and energy absorption of the Ce/Cr coated alloy foams are strongly affected by the Ce addition. Especially, the yield stress and plateau stress of 2% Ce/Cr coated alloy foam are approximately 2 times as high as those of the Ni−Cr−Fe alloy foam substrate in Table 4.

3.7 Deformation and failure analysis

For further insight into the deformation mechanisms of Ce/Cr coated Ni−Cr−Fe alloy foams, the microstructures of the Ce/Cr coated alloy foams are analyzed with different strain points. In the corresponding stress–strain curves in Fig. 12(a), the stress–strain points are denoted in Figs. 12(b)−(e), respectively. Firstly, the cell is still in the elastic regime and there is no visible plastic deformation at a strain of 0.06 (Fig. 12(b)). After further loading to a strain of 0.1,

Table 4 Mechanical properties of bare Ni−Cr−Fe alloy foam and Ce/Cr coated alloy foams

Foam	Relative density/%	Microhardness values (VHN)	Yield stress/MPa	Plateau stress/MPa	Energy absorption/ ($MJ \cdot m^{-3}$)
Ni−Cr−Fe	8.1	210±10	4.2±0.5	2.2±1	3.6±0.5
1% Ce/Cr coated	8.4	220±10	4.8±1	2.8±1.5	4.3±1
2% Ce/Cr coated	8.4	260±5	7.2±1	2.3±1.5	6.4±1
2% Ce/Cr coated	8.6	270±5	8.9±1	3.7±1.5	7.3±1
3% Ce/Cr coated	8.5	230±5	5.6±1	1.5±1.5	4.5±1

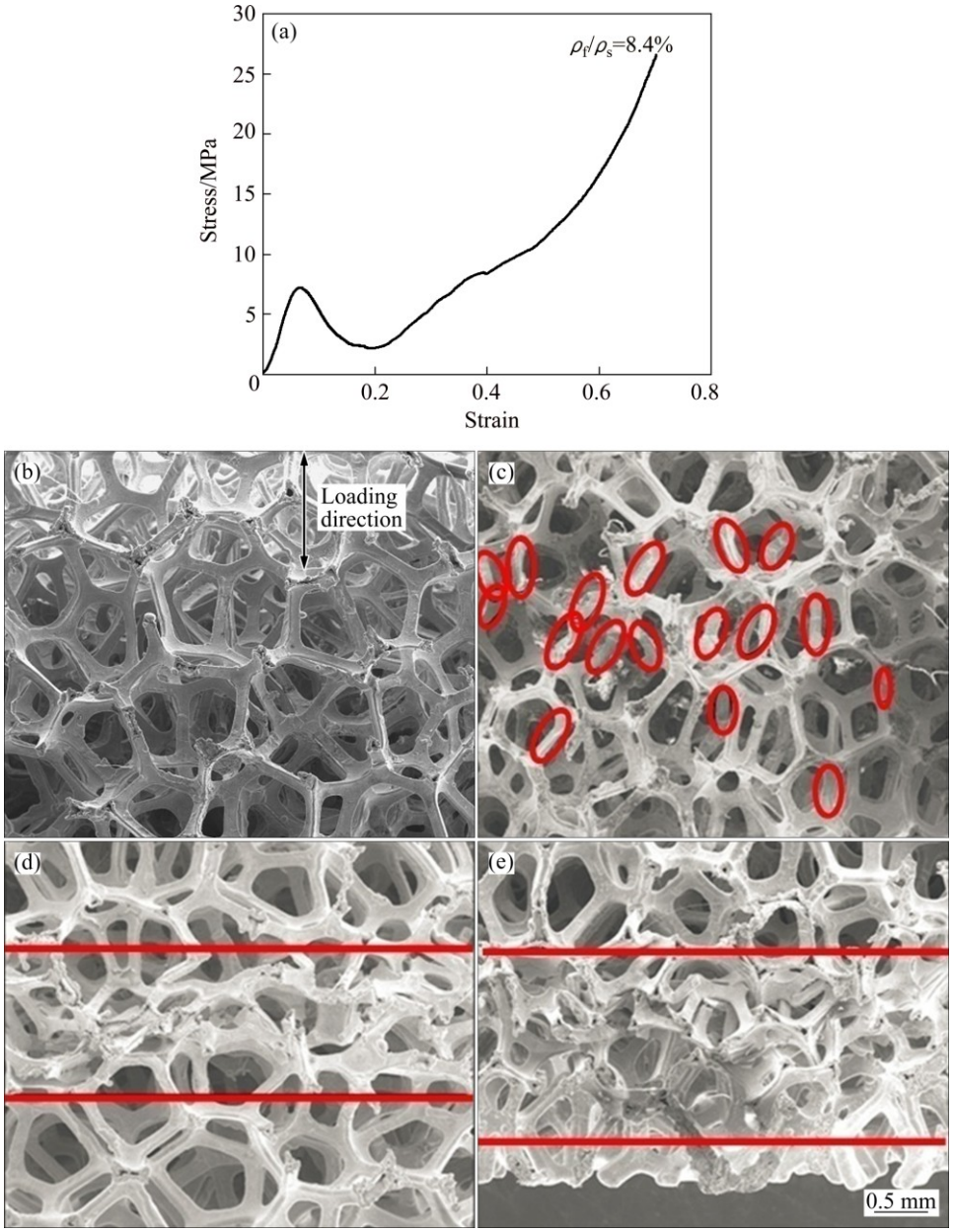

Fig. 12 Strain−stress curve (a) and morphologies (b−e) of 2% Ce/Cr coated Ni−Cr−Fe alloy foams with different strains: (b) ε=0.06; (c) ε=0.2; (d) ε=0.3; (e) ε=0.5

the struts bend further and buckle progressively. When the stress reaches the yield point of alloy foams, the peak stress represents the maximum fracture resistance of the Ce/Cr coated alloy foams. After the peak stress is reached, the stress decreases rapidly as a result of increasing strain and reaches the low valley stress in Fig. 12(a), which suggests the onset of the fracture of cell walls under the local bending moment. The Ce/Cr coated alloy foams undergo mechanical failure and the cracking of strut is observed at a strain of 0.2 in Fig. 12(c).

With further deformation, the progressive collapse of unit cell walls results in the nearly constant plateau stage. The successive collapse of the foam happens to the weakest foam structure layer (the middle layer) at a strain ε=0.3 in Fig. 12(d). Then, a layer by layer failure owing to the bending of cell walls is apparent [28], and more and more cell-walls experience plastic strain and fracture, which can be found throughout the whole specimen in Fig. 12(e). Finally, the Ce/Cr coated alloy foam reaches the densification stage.

Figure 13 shows the high magnification SEM images of the 2% Ce/Cr coated Ni−Cr−Fe alloy cell walls with strains of 0.2, 0.3 and 0.5. It is obvious that

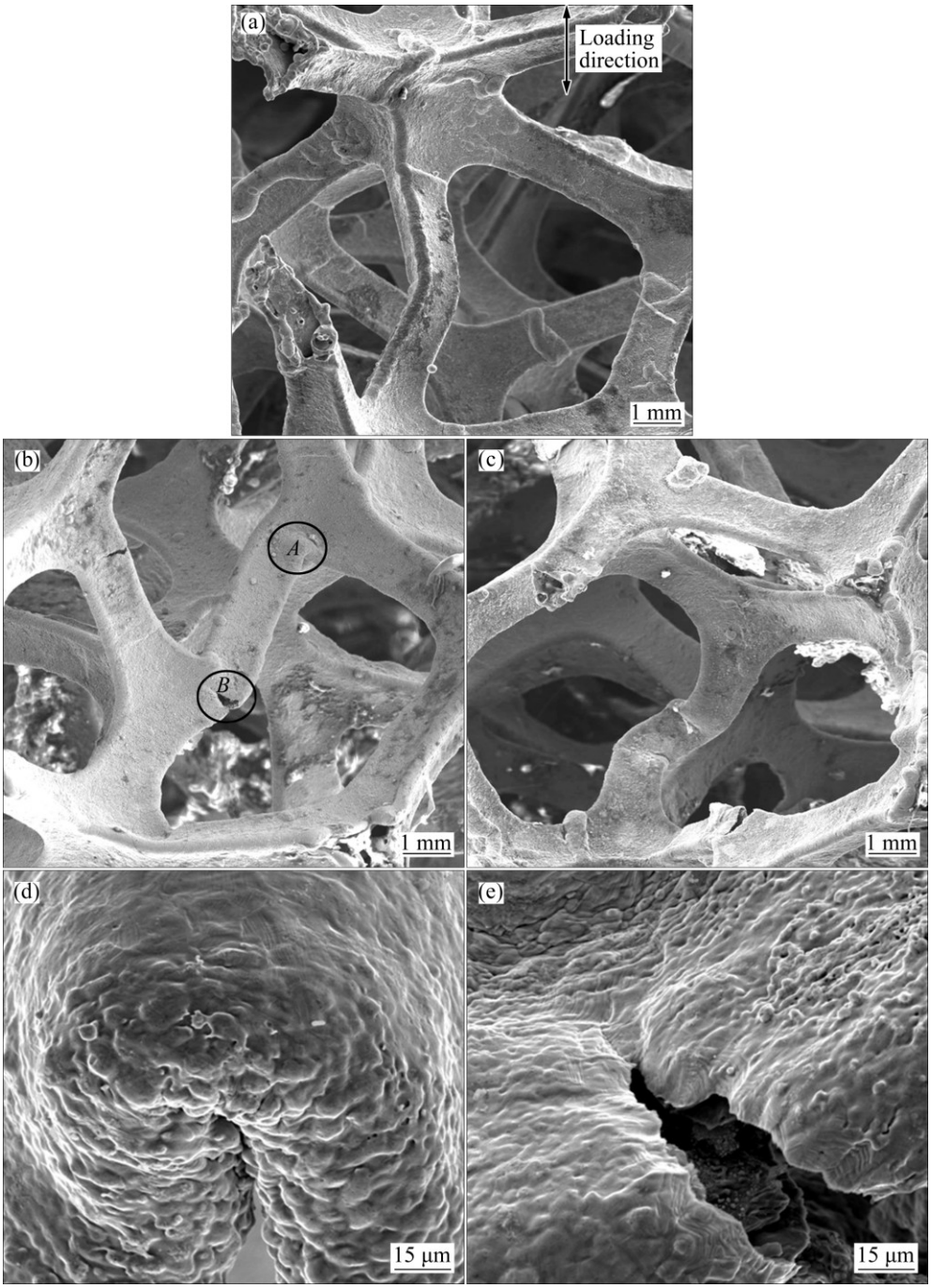

Fig. 13 Deformation morphologies of 2% Ce/Cr coated Ni−Cr−Fe alloy cell walls: (a) ε=0.2; (b) ε=0.3; (c) ε=0.5; (d, e) Enlarged images of zones *A* and *B* in Fig. 13(b), respectively

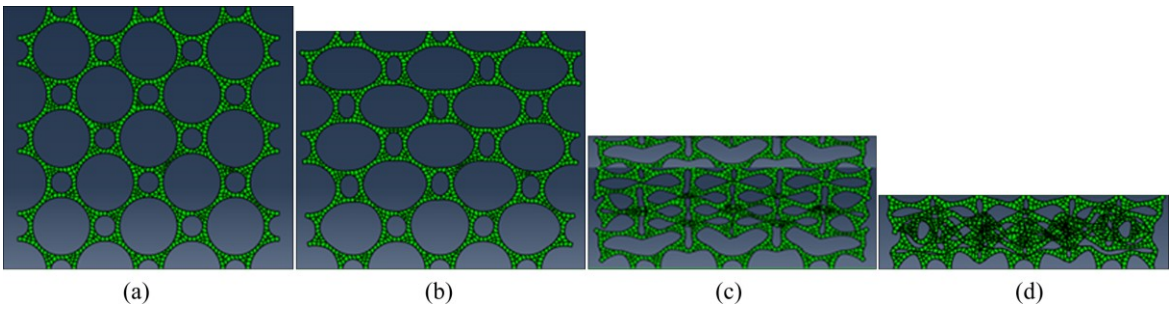

Fig. 14 Compressive behavior of 2% Ce/Cr coated Ni−Cr−Fe alloy cell walls obtained by image-based FE analysis: (a) ε=0.06; (b) ε=0.2; (c) ε=0.3; (d) ε=0.5

the distortion and cracking are the main deformation behavior of the Ce/Cr coated alloy foam under the compression state. At first, deformation usually occurs in the middle of the foam skeleton with a strain of 0.2, and a great number of micro-fatigue-cracks occur in unit cell wall of the Ce/Cr coated alloy foam in Fig. 13(a) (Points *A* and *B*). Then, many cracks and wrinkles appear on the nodes of the alloy cell walls with a strain of 0.3 in Fig. 13(b), and the crack edges appear to be irregular, which is a natural result of the ductile fracture mechanism. With further increasing the pressure, the deformation process happens in the other plane, which is perpendicular to the loading direction with a strain of 0.5 in Fig. 13(c). Because the porosity is as high as 91.4%−91.6%, the majority of cell walls are subjected to bending deformation.

3.8 Simulation results and validation

Figure 14 demonstrates the FE predictions of the whole deformation process of the Ce/Cr coated alloy foams at various strain stages (ε=0.06−0.5). It can be seen that the predicted results exhibit the collapse and the plastic deformation of the Ce/Cr coated alloy foams, which are in agreement with the experimental data (Figs. 12 and 13). As can be seen, firstly the cells undergo slight elastic−plastic deformation in the range of ε=0.06−0.2. The deformation begins in the middle layer of the specimens. Then, the cell walls in this layer undergo severe deformation at a strain of 0.3. Finally, the coated alloy foam undergoes a certain degree of deformation at a strain of 0.5. Therefore, it is possible to predict that the deformation of Ce/Cr coated alloy foam firstly occurs in the middle layer. Subsequently, the deformation expands from the middle to the edge of the coated alloy foam specimen.

4 Conclusions

1) With the addition of Ce, the microstructure of the 2% Ce/Cr coated Ni−Cr−Fe alloy foams is denser and more uniform. The yield stress and the plateau stress of the 2% Ce/Cr coated alloy foams are increased significantly. Simultaneously, according to the Gibson and Ashby model, the compressive strength of the Ce/Cr coated alloy foams is increased, as compared with a hypothetical Ni−Cr−Fe alloy foam.

2) With the increase of Ce content from 1% to 3%, the microhardness value of the Ce/Cr coated alloy foams firstly increases and then decreases. The Ce/Cr coatings significantly increase both the strength and energy absorption of the coated alloy foams. Especially, the average energy-absorption performance of 2% Ce/Cr coated alloy foam is 1.9 times as high as that of the bare Ni−Cr−Fe alloy foam.

3) The distortion and cracking are the main deformation behavior of the Ce/Cr coated alloy foam under the quasi-static compression. At first, the cells of the coated alloy foam undergo slight elastic-plastic deformation. Then, many cracks and wrinkles appear on the nodes of the alloy cell walls. With continuing to increase the pressure, the deformation process happens in the other plane which perpendicular the loading direction. The collapse proceeds step by step with further increasing the pressure. Simultaneously, the compressive behavior of FE predictions is in agreement with the experimental results.

References

[1] BANHART J. Manufacture, characterization and application of cellular metals and metal foams [J]. Progress in Materials Science, 2001, 46: 559−632.

[2] ASHBY M F, EVANS A G, FLECK N A, GIBSON L J, HUTCHINSON J W, WADLEY H N G. Metal foams—A design guide [M]. Boston: Butterworth−Heinemann, 2000.

[3] MUTLU I. Synthesis and characterization of Ti−Co alloy foam for biomedical applications [J]. Transactions of Nonferrous Metals Society of China, 2016, 26: 126−137.

[4] PANG Qiu, WU Gao-hui, SUN Dong-li, XIU Zi-yang, ZHANG Qiang, HU Zhi-li. Compressive property and energy absorption characteristic of 3D open-cell Ni−Cr−Fe alloy foams under quasi-static conditions [J]. Transactions of Nonferrous Metals Society of China, 2012, 22: 566−572.

[5] YUAN Jian-yu, LI Yan-xiang. Effects of cell wall property on compressive performance of aluminum foams [J]. Transactions of Nonferrous Metals Society of China, 2015, 25: 1619−1625.

[6] CHOE H, DUNAND D C. Synthesis, structure, and mechanical

properties of Ni−Al and Ni−Cr−Al superalloy foams [J]. Acta Materialia, 2004, 52: 1283−1295.
[7] BOONYONGMANEERAT Y, SCHUH C A, DUNAND D C. Mechanical properties of reticulated aluminum foams with electrodeposited Ni−W coatings [J]. Scripta Materialia, 2008, 59: 336−339.
[8] CHOE H, DUNAND D C. Mechanical properties of oxidation-resistant Ni−Cr foams [J]. Materials Science and Engineering A, 2004, 384: 184−193.
[9] HODGE A M, DUNAND D C. Synthesis of nickel−aluminide foams by pack-aluminization of nickel foams [J]. Intermetallics, 2001, 9: 581−589.
[10] TUCKER J D, NAJAFABADI R, ALLEN T R, MORGAN D. *Ab* initio-based diffusion theory and tracer diffusion in Ni−Cr and Ni−Fe alloys [J]. Journal of Nuclear Materials, 2010, 405: 216−234.
[11] WANG Y, CHEN W. Microstructures, properties and high-temperature carburization resistances of HVOF thermal sprayed NiAl intermetallic-based alloy coatings [J]. Surface & Coatings Technology, 2004, 183: 18−28.
[12] PANG Qiu, HU Zhi-li, ZHANG Rong, ZUO Xiao-qiong, WU Gao-hui. Effects of rare earth modified Cr coating on structure and oxidation resistance of open-cell Ni−Cr−Fe alloy foam [J]. Rare Metal Materials and Engineering, 2016, 45: 1826−1831.
[13] PANG Q, WU G H, SUN D L, XIU Z Y, JIANG L T. A dual-layer Ce−Cr/Al oxidation resistant coating for 3D open-cell nickel based foams by a two-step pack cementation [J]. Materials Science and Engineering A, 2013, 568: 228−238.
[14] PANG Q, WU G H, XIU Z Y, JIANG L T, SUN D L. Microstructure, oxidation resistance and high-temperature strength of a new class of 3D open–cell nickel-based foams [J]. Materials Characterization, 2012, 70: 125−136.
[15] HOU Q Y, WANG J T. Influence of CeO_2 on the microstructure and wear resistance of iron-based alloy coating studied by Rietveld refinement method [J]. Surface & Coatings Technology, 2010, 204: 2677−2682.
[16] WANG Bin, HE De-ping, SHU Guang-ji. Compressive property and energy absorption of foamed Al alloy [J]. Acta Metallurgica Sinica, 2000, 36: 1037−1040.
[17] XUE Xiao-bing, WANG Li-qiang, WANG Min-min, LÜ Wei-jie, ZHANG Di. Manufacturing, compressive behaviour and elastic modulus of Ti matrix syntactic foam fabricated by powder metallurgy [J]. Transactions of Nonferrous Metals Society of China, 2012, 22: 188−192.
[18] YUAN Jian-yu, LI Yan-xiang. Effects of cell wall property on compressive performance of aluminum foams [J]. Transactions of Nonferrous Metals Society of China, 2015, 25: 1619−1625.
[19] HOU Guang-ya, WU Chao-shan, TANG Yi-ping, SUN Lu-yang, CAO Hua-zhen, ZHENG Guo-qu. Effects of surface aluminizing on structure and compressive strength of Fe foam prepared by electrodeposition [J]. Materials Science and Engineering A, 2014, 602: 33−40.
[20] LI Bin-chao, ZHAO Gui-ping, LU Tian-jian. Low strain rate compressive behavior of high porosity closed-cell aluminum foams [J]. Chinese Journal of Theoretical and Applied Mechanics, 2011, 43: 122−135. (in Chinese)
[21] YU H J, GUO Z Q, LI B, YAO G C, LUO H J, LIU Y H. Research into the effect of cell diameter of aluminum foam on its compressive and energy absorption properties [J]. Materials Science and Engineering A, 2007, 454: 542−546.
[22] RAJAK D K, KUMARASWAMIDHAS L A, DAS S, KUMARAN S S. Characterization and analysis of compression load behaviour of aluminium alloy foam under the diverse strain rate [J]. Journal of Alloys and Compounds, 2016, 656: 218−225.
[23] PERONI L, SCAPIN M, FICHERA C, LEHMHUS D, WEISE J, BAUMEISTER J, AVALLE M. Investigation of the mechanical behaviour of AISI 316L stainless steel syntactic foams at different strain-rates [J]. Composites (Part B), 2014, 66: 430−442.
[24] GIBSON L J, ASHBY M F. Cellular solids-structure and properties [M]. Cambridge: Cambridge University Press, 1997.
[25] MINDLIN H. Aerospace structural metals handbook [M]. New York: Syracuse University Press, 1997.
[26] BOONYONGMANEERAT Y, DUNAND D C. Ni−Mo−Cr foams processed by casting replication of sodium aluminate preforms [J]. Advanced Engineering Materials, 2008, 10: 379−383.
[27] LI Y G, WEI Y H, HOU L F, GUO C L, YANG S Q. Fabrication and compressive behaviour of an aluminium foam composite [J]. Journal of Alloys and Compounds, 2015, 649: 76−81.
[28] KADKHODAPOUR J, MONTAZERIAN H, SAMADI M, SCHMAUDER S, MEHRIZI A A. Plastic deformation and compressive mechanical properties of hollow sphere aluminum foams produced by space holder technique [J]. Materials & Design, 2015, 83: 352−362.

Ce 含量对 Ce/Cr 涂层开孔 Ni−Cr−Fe 泡沫合金力学性能的影响

庞 秋[1,2]，胡志力[2,3,4]，王国荣[1]

1. 武汉东湖学院 机电工程学院，武汉 430212；
2. 武汉理工大学 现代汽车零部件湖北省重点实验室，武汉 430070；
3. 武汉理工大学 汽车零部件技术湖北省协同创新中心，武汉 430070；
4. 哈尔滨工业大学 先进焊接及连接国家重点实验室，哈尔滨 150001

摘 要：采用固体粉末包埋工艺将 Ce/Cr 涂层均匀分布在开孔 Ni−Cr−Fe 泡沫合金表面。利用静态压缩试验对 Ce/Cr 涂层改性 Ni−Cr−Fe 泡沫合金的力学性能进行研究。同时，对静态压缩条件下 Ce/Cr 涂层 Ni−Cr−Fe 泡沫合金的变形和破坏机制进行讨论。研究结果表明：添加不同含量的 CeO_2 粉对 Ce/Cr 涂层泡沫合金力学性能产生较大影响。虽然与初始 Ni−Cr−Fe 泡沫合金相比密度增加，但是 Ce/Cr 涂层泡沫合金的屈服强度和能量吸收性能明显提高。尤其 2%Ce/Cr(质量分数)涂层泡沫合金的能量吸收性能为初始 Ni−Cr−Fe 泡沫合金的 1.9 倍。此外，Ce/Cr 涂层泡沫合金的力学性能随着应变速率的增加而增加。扫描电子显微镜(SEM)观察显示变形和开裂是 Ce/Cr 涂层泡沫合金主要的变形行为。

关键词：镍基泡沫合金；力学性能；屈服应力；平台应力；失效机制

(Edited by Wei-ping CHEN)